Electronic Supplementary Information for

Impact of Quantum Dot Purification Methods on Sensing Performance for Heavy Metal Detection in Environmental Pollution Monitoring

Laura A. Rojas-Palomino,[a] Cristian Blanco-Tirado,[a] and Marianny Y. Combariza,[a] Carlos A. Martínez-Bonilla[b*]

[a] *Centro de Estudios e Investigaciones Ambientales – CEIAM, Universidad Industrial de Santander, Bucaramanga Colombia.*
[b] *Département de Chimie, Université de Montréal, C.P. 6128, Succ. Centre-ville, Montreal, QC, H3C 3J7, Canada.*
[c] *Grupo de Investigación de Fisicoquímica Teórica y Experimental – GIFTEX, Universidad Industrial de Santander, Bucaramanga Colombia.*

Present address: Département de Chimie, Université de Montréal, C.P. 6128, Succ. Centre-ville, Montreal, QC, H3C 3J7, Canada.

Corresponding author e-mail: camartinez885@gmail.com, carlos.andres.martinez.bonilla@umontreal.ca

Table of Contents **Pages**

1. **Heavy Metals** S2
2. **XPS general composition data.** S2
3. **Dialysis performance.** S3
4. **Silica column performance.** S4
5. **Nuclear magnetic resonance (NMR) of the fraction purified by column.** S5
6. **Quantum yield calculation.** S7
7. **ICP-OES performance.** S14
8. **Emission of TEMPO-oxidized cellulose nanofibers (TOCN)** S15
9. **Stern-Volmer for fluorescence quenching of composites by Hg^{2+} ions.** S16

1. Heavy Metals

For the evaluation of the CQDs, heavy metal ion solutions were prepared at a concentration of 0.1 M, as detailed in Table S1. This table lists the specific cation evaluated, the corresponding salt used for its preparation, and the commercial supplier of each reagent.

Table S1. *Heavy Metal salts, corresponding cations, and suppliers for 0.1 M solutions*

Metal Cation	***Salt Used***	***Chemical Formula***	***Commercial Supplier***
Mercury (Hg^{2+})	*Mercury(II) chloride*	*$HgCl_2$*	*Sigma-Aldrich*
Cadmium (Cd^{2+})	*Cadmium(II) chloride*	*$CdCl_2$*	*Sigma-Aldrich*
Silver (Ag^{+})	*Silver nitrate*	*$AgNO_3$*	*Merck*
Lead (Pb^{2+})	*Lead(II) chloride*	*$PbCl_2$*	*Sigma-Aldrich*
Copper (Cu^{2+})	*Copper(II) nitrate tetrahydrate*	*$Cu(NO_3)_2{\cdot}4H_2O$*	*Merck*
Nickel (Ni^{2+})	*Nickel(II) nitrate hexahydrate*	*$Ni(NO_3)_2{\cdot}6H_2O$*	*Sigma-Aldrich*
Cobalt (Co^{2+})	*Cobalt(II) nitrate hexahydrate*	*$Co(NO_3)_2{\cdot}6H_2O$*	*Sigma-Aldrich*

2. XPS general composition data.

The XPS analysis provides a detailed characterization of the sample's surface composition. This section presents the general elemental composition, peak positions, full width at half maximum (FWHM), and atomic percentages obtained from the deconvoluted spectra. Additionally, the raw data is included to ensure transparency and reproducibility of the results.

Table S2. Elemental composition of both types of CQDs

	Carbon (%)	***Oxygen (%)***	***Nitrogen (%)***	***Total (%)***
CQDs-CC	*70*	*25*	*4.9*	*99.9*
CQDs-DL	*66*	*27*	*5.8*	*98.8*

Table S3. *XPS general composition data obtained from different samples.*

Sample	Name	Position	FWHM	Raw Area	%At Conc
CQDs-DL	C 1s	284.8	3.0	67433.9	66.8
	O 1s	531.8	3.4	66911.6	27.4
	N 1s	400.8	3.1	9608.1	5.8
CQDs-CC	C 1s	284.8	3.1	60421.5	70.1
	O 1s	531.8	3.5	51858.9	24.9
	N 1s	399.8	3.0	7041.8	5.0

BNC	C 1s	284.8	3.6	139501.2	62.9
	O 1s	531.8	2.8	85079.5	37.1
	N 1s	-	-	-	-
TOCN	C 1s	284.8	3.4	85780.7	38.6
	O 1s	531.8	2.5	141040.3	61.4
	N 1s	-	-	-	-
Biocomposite	C 1s	284.8	4.2	117102.2	53.6
	O 1s	531.8	2.8	102555.7	45.3
	N 1s	381.8	2.6	1071.8	1.2

3. Dialysis purification.

Figure S1 illustrates the physical and spectral changes observed during the dialysis process. Figure S1(a), (b), and (c) depict the initial physical appearance of the system at time 0, immediately upon contact with water. Figure S1 (d) and (e) show the physical state of the dialysis setup after 72 hours, highlighting the observable changes in fluorescence intensity over time. Figure S1 (f) presents the emission spectra of both the dialysate water changes and the dialyzed product (CQDs-DL), demonstrating that the most fluorescent families of CQDs migrate first, resulting in the dialyzed product exhibiting significantly reduced fluorescence emission. Finally, Figure S1 (g) displays the physical appearance of the water changes and the CQDs-DL product under 365 nm UV light, further emphasizing the fluorescence characteristics after dialysis.

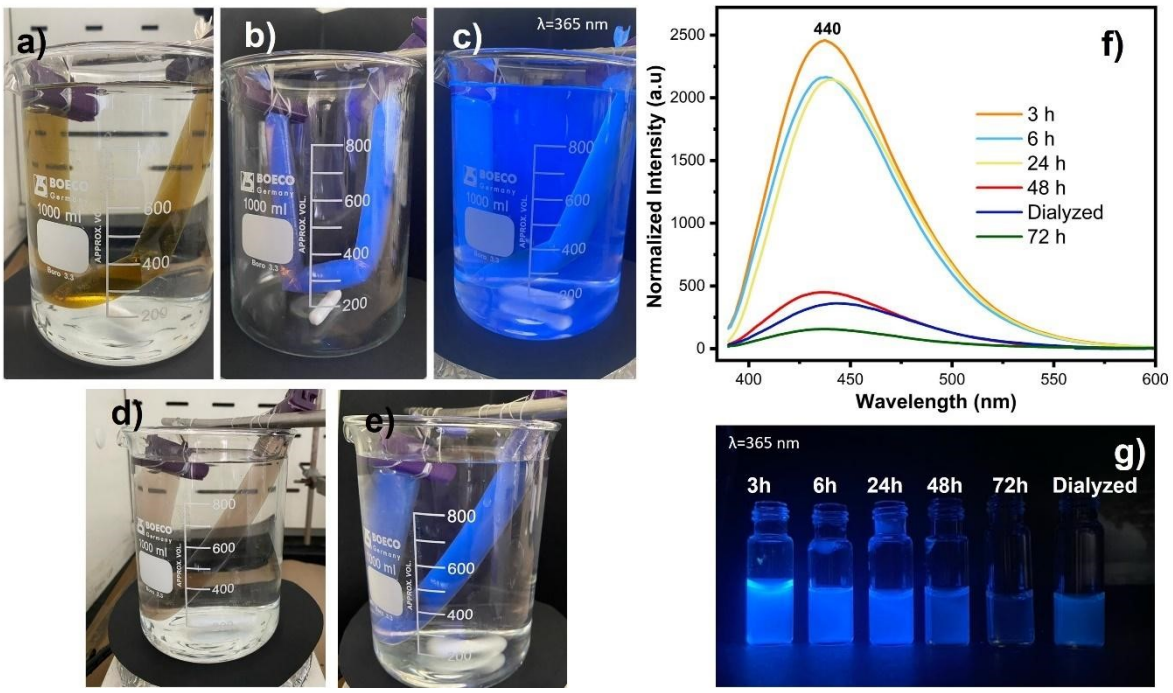

Figure S 1. *Dialysis Performance. a) Physical aspect of the first contact of the dialysis membrane with water under natural light and b,c) UV light of 365 nm.d) Physical aspect at 72h of the dialysis membrane under natural light and g) UV light of 365 nm. h) Emission spectra of water changes and dialyzed product, i) Physical aspect of water changes and dialyzed product under UV light of 365 nm.*

4. Column Chromatography purification.

Figures S2(a), S2(b) and S2(c) illustrate the purification process using column chromatography with silica powder (60 Å) as the stationary phase. The crude reaction mixture was dried using rotary evaporation, dissolved in 3 mL of ethanol, and adsorbed onto silica (approximately 0.8 g). The mixture was then poured onto the wet column. Elution initiated with ethyl acetate (fraction 1), followed by a mixture of ethyl acetate and ethanol in ratios of 1:1, 1:3, and 1:5 (fraction 2 to 4). The sequence continued with ethanol (fraction 5), and culminated in a mixture of ethanol and water at a ratio of 1:1 (fraction 6). As shown in Figure S2(e), six distinct fractions were obtained during the elution process. Thin-layer chromatography (TLC) analysis, presented in Figure S2(f), confirmed the emissive properties of each fraction, identifying fraction #5 as the most fluorescent. This fraction was selected as the purified sample for subsequent characterization and further experimentation.

Figure S 2. *Silica column performance. a) Reaction crude under natural light, b) reaction crude under UV light 365 nm, c) reaction crude dried, d) silica column assembly, e) fractions obtained, f) TLC of fractions obtained.*

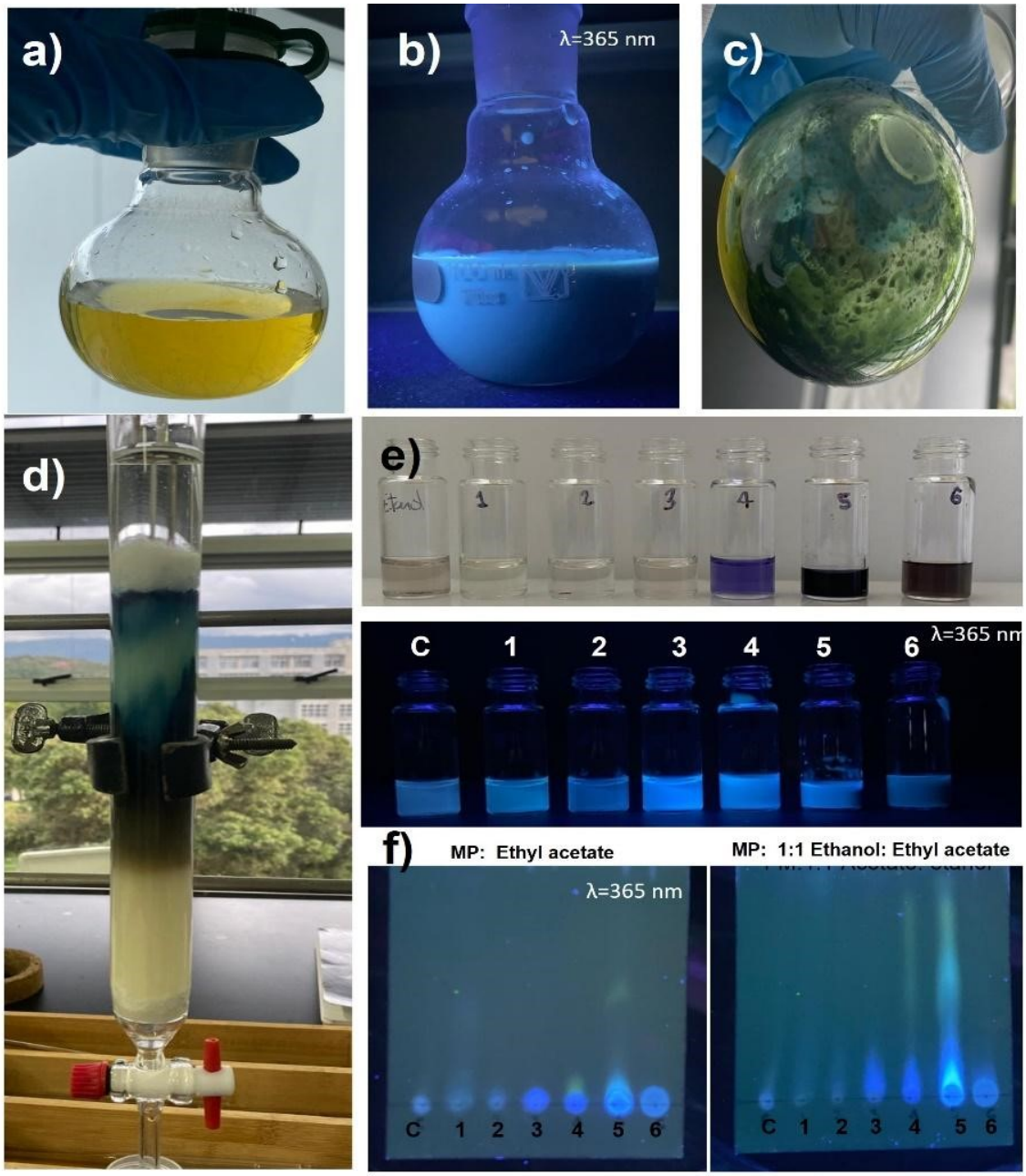

5. Nuclear magnetic resonance (NMR) of the fraction purified by column.

The NMR spectra provide detailed insights into the structural characteristics of the purified fraction (CQDs-CC) obtained via silica column chromatography. The analysis includes the ^{1}H NMR spectrum (Figure S3), which reveals high-field signals characteristic of saturated compounds with minimal quaternary hydrogens. The overlay of the ^{13}C and DEPT-135 spectra (Figure S4) further elucidates the nature of the carbons present, confirming both sp^2 and sp^3 hybridizations.[1] Finally, the HSQC spectrum (Figure S5) highlights the interactions between carbons and hydrogens, offering a comprehensive understanding of the molecular framework of the purified fraction.

Figure S3. *^{1}H spectrum of the purified fraction of CQDs-CC.*

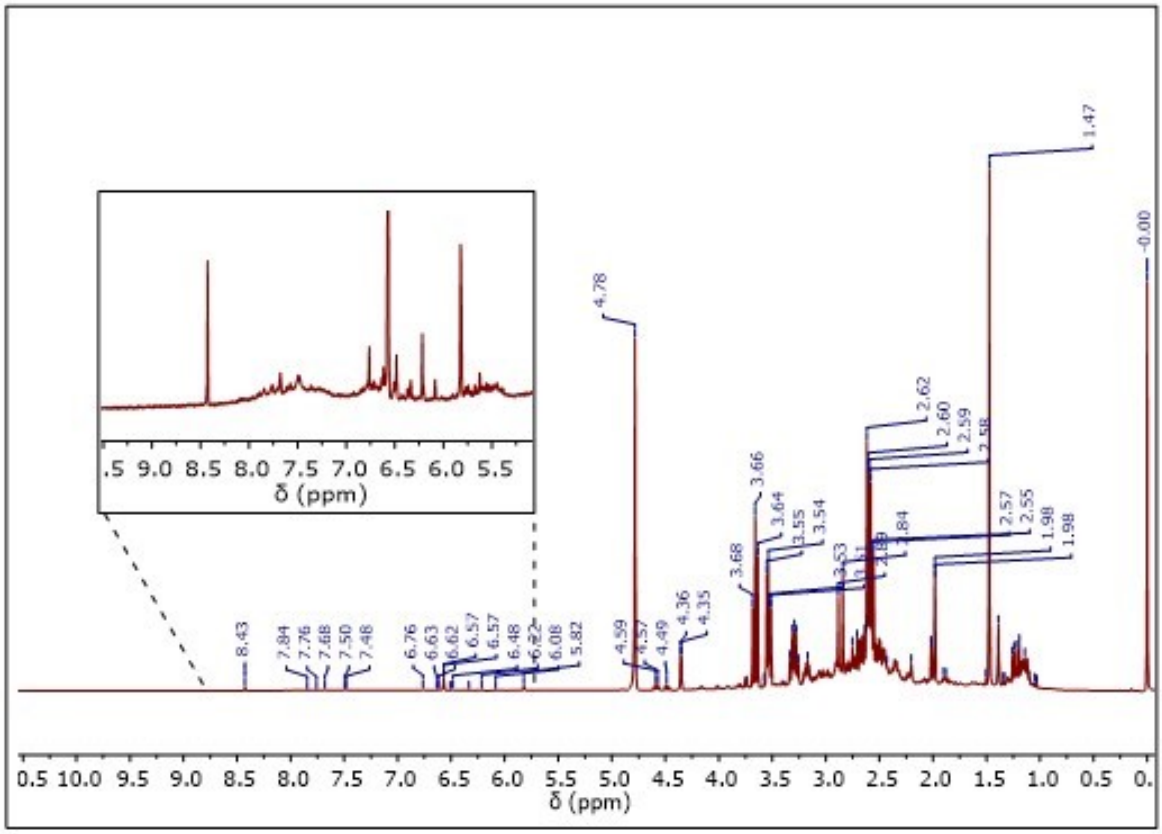

Figure S 4. *^{13}C, DEPT135 overlap spectrum of the purified fraction of CQDs-CC.*

Figure S 5. *HSQC spectrum of the purified fraction of CQDs-CC.*

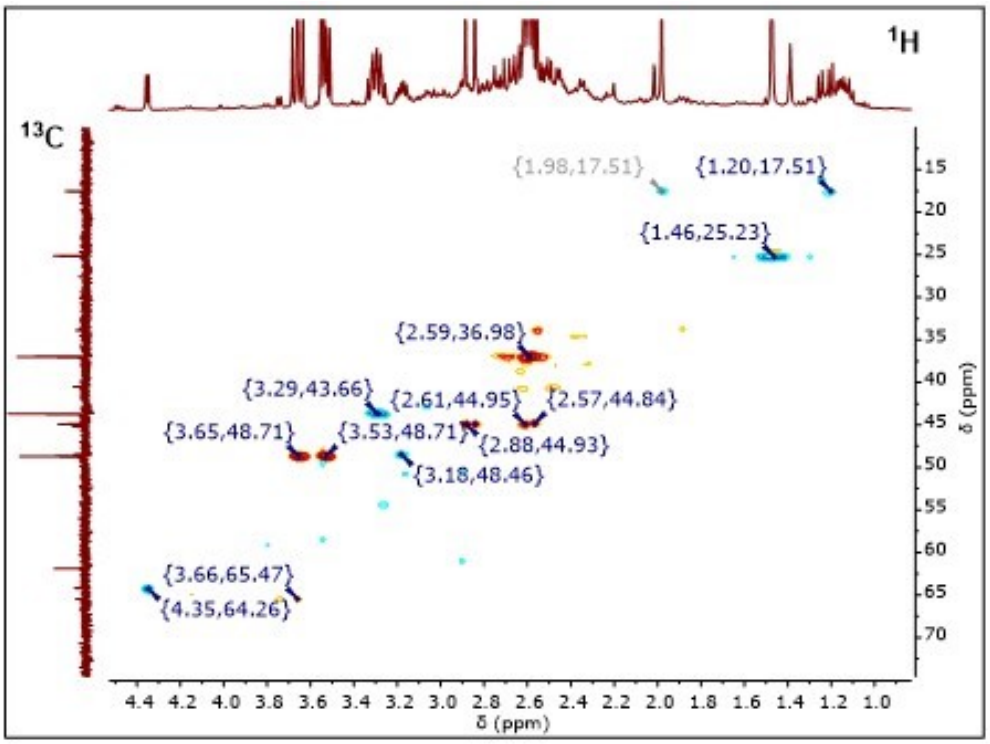

6. Quantum yield calculation

QY was calculated using the comparative method. Standard reference materials, such as rhodamine 6G, rhodamine B, and quinine sulfate, were used as calibration standards. The consolidated QY values for the samples, calculated in relation to the rhodamine 6G theoretical QY value of 0.95, are presented in Table S4. For each standard and CQDs sample, absorbance data and the integrated emission area from the fluorescence spectra were obtained at varying concentrations. In the comparative method, QY is calculated using the slope of the line determined from the plot of the absorbance against the integrated fluorescence intensities.[2] The QY was then calculated using the following equation:

$$\Phi = \Phi r.\frac{m\, n^2}{m_r n_r^2}$$

Where Φ is the quantum yield, m is the slope of the line obtained from the plot of the integrated fluorescence intensity vs. absorbance. n is the refractive index of the solvent, and the subscript r refers to the reference fluorophore of known QY. The results for the QY of the standards and the evaluated CQD samples are presented below, providing a comprehensive overview of their optical performance.

Table S 4. *QY obtained from the different samples*

Sample	QY
ROD 6G	0.95
ROD B	0.71
Quinine sulfate	0.54
CQDs-CC	0.47
CQDs-DL	0.05

Figure S 6. *6G rhodamine pattern used for QY calculation.*

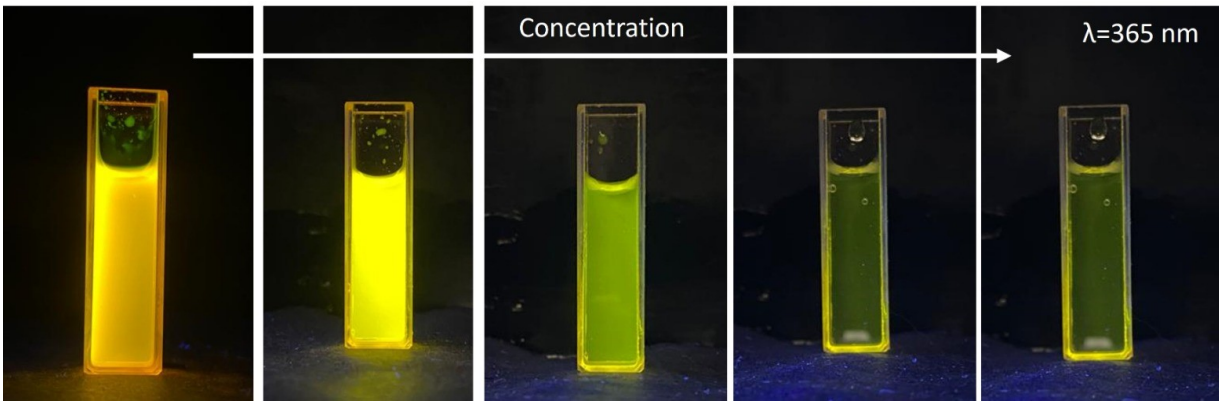

Concentration (mol/L)	Abs at 530 nm	Integrated fluorescence area
$1.75x10^{-6}$	0.128	951769.363
$1.35x10^{-6}$	0.098	799580.976
$1x10^{-6}$	0.066	579305.589
$6x10^{-7}$	0.040	365358.315
$2x10^{-7}$	0.014	152618.775

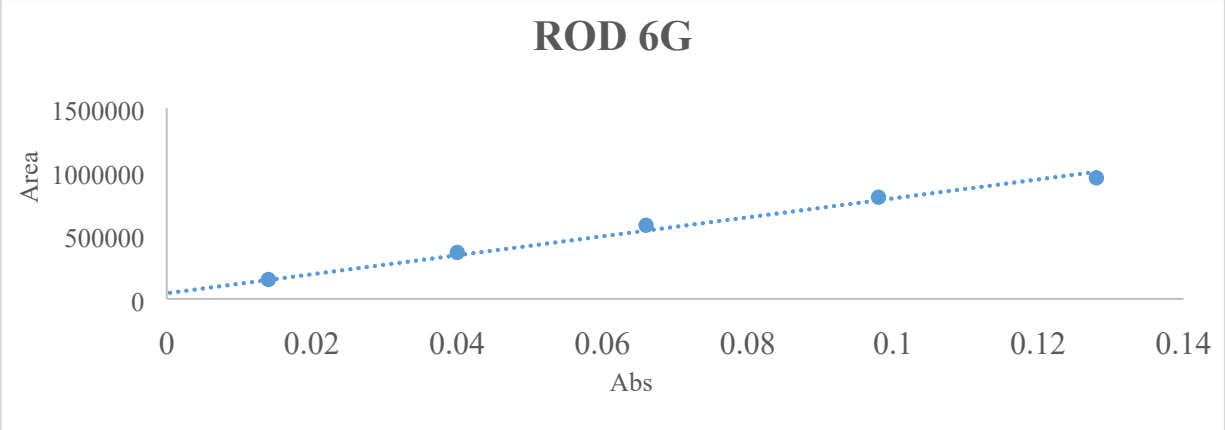

Figure S 7. *Rhodamine B pattern used for QY calculation*

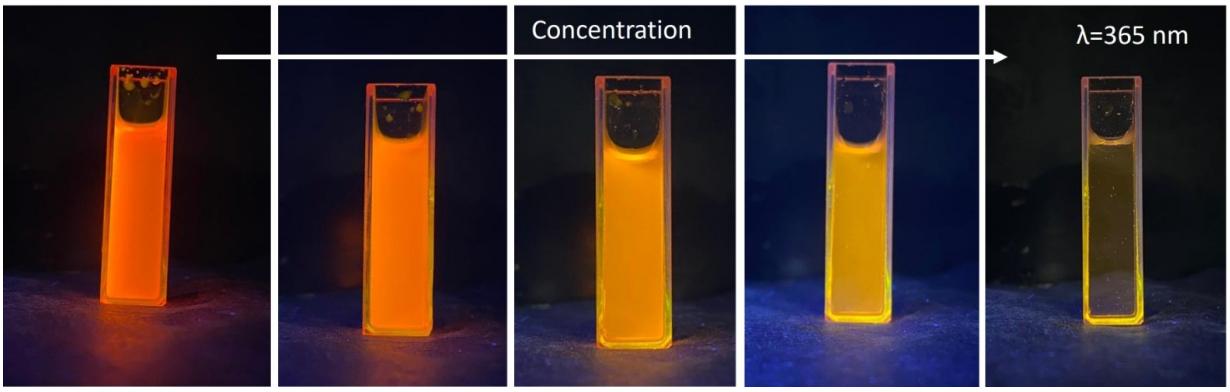

Concentration (mol/L)	Abs at 545 nm	Integrated fluorescence area
$8x10^{-7}$	0.070	381182.706
$6x10^{-7}$	0.052	307329.951
$4x10^{-7}$	0.036	240398.194
$2x10^{-7}$	0.019	123358.096
$1x10^{-7}$	0.010	58412.518

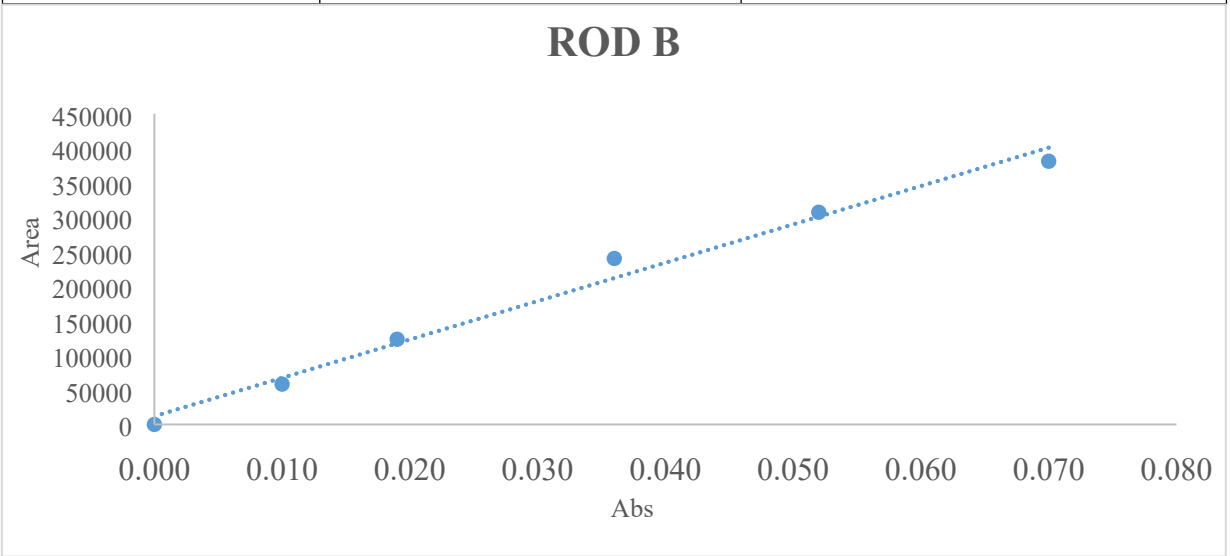

Figure S8. *Quinine sulfate pattern used for QY calculation*

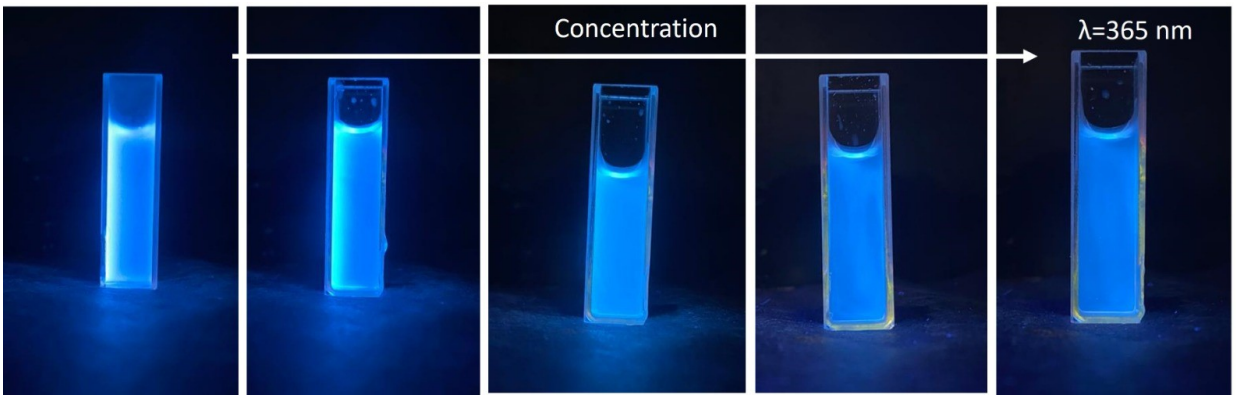

Concentration (mol/L)	Abs at 350 nm	Integrated fluorescence area
$8x10^{-7}$	0.081	500873.070
$6x10^{-7}$	0.053	362563.383
$4x10^{-7}$	0.030	215368.739
$2x10^{-7}$	0.016	152285.930
$1x10^{-7}$	0.006	82786.782

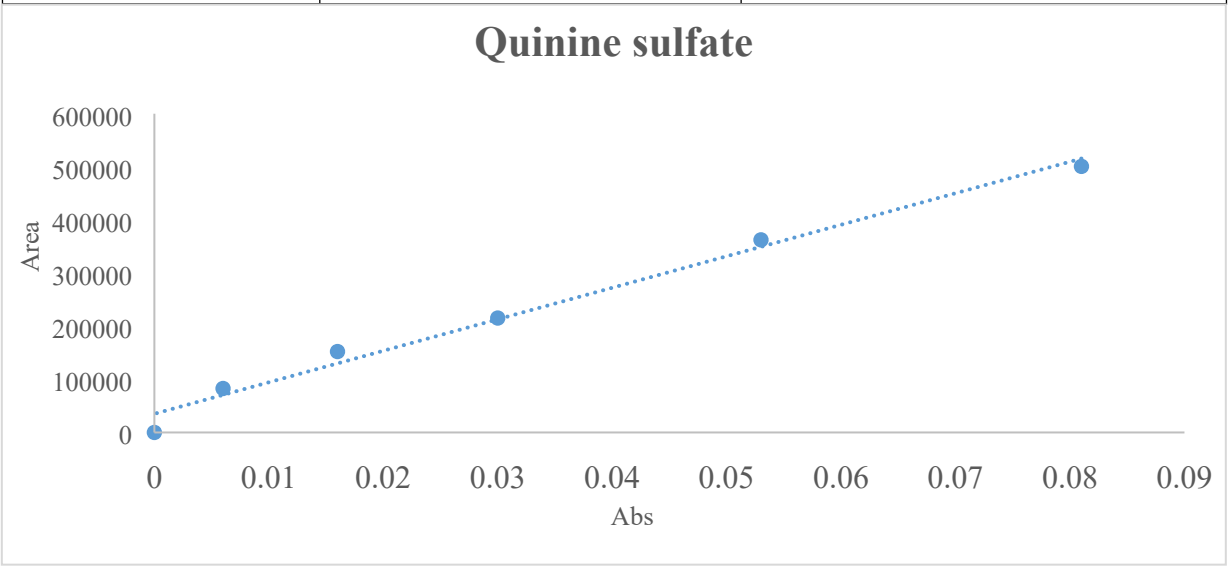

***Figure S 9**. CQDs- CC used for QY calculation*

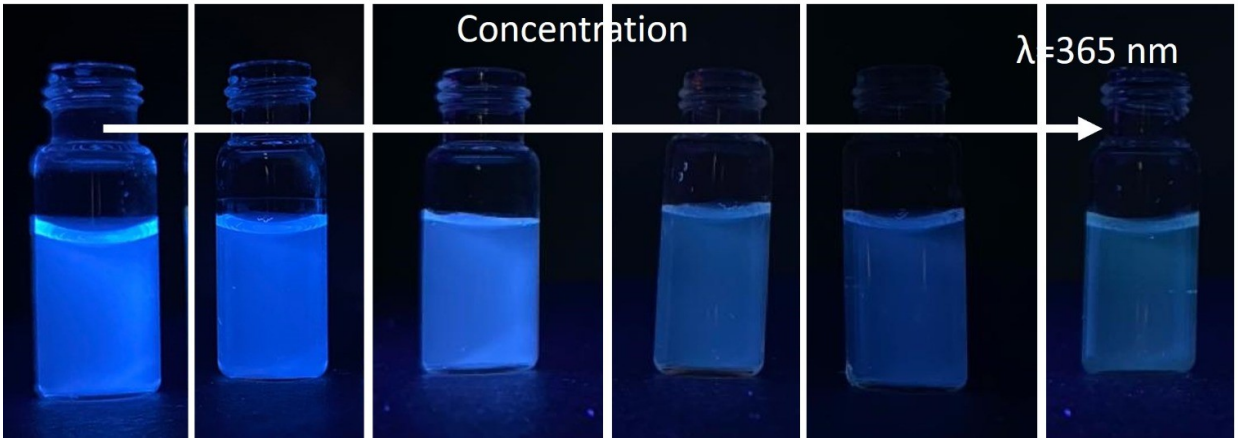

Concentration (mg/L)	Abs at 335 nm	Integrated fluorescence area
150	0.094	483468.469
100	0.057	333849.818
50	0.028	173328.122
30	0.019	109690.470
8	0.003	28913.524

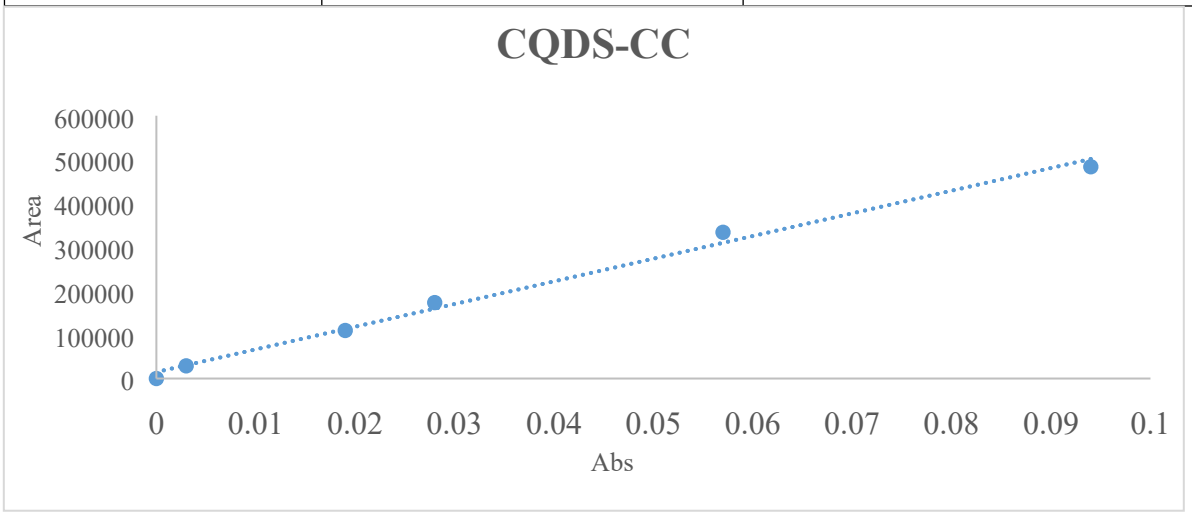

Figure S 10. *CQDs - DL used for QY calculation*

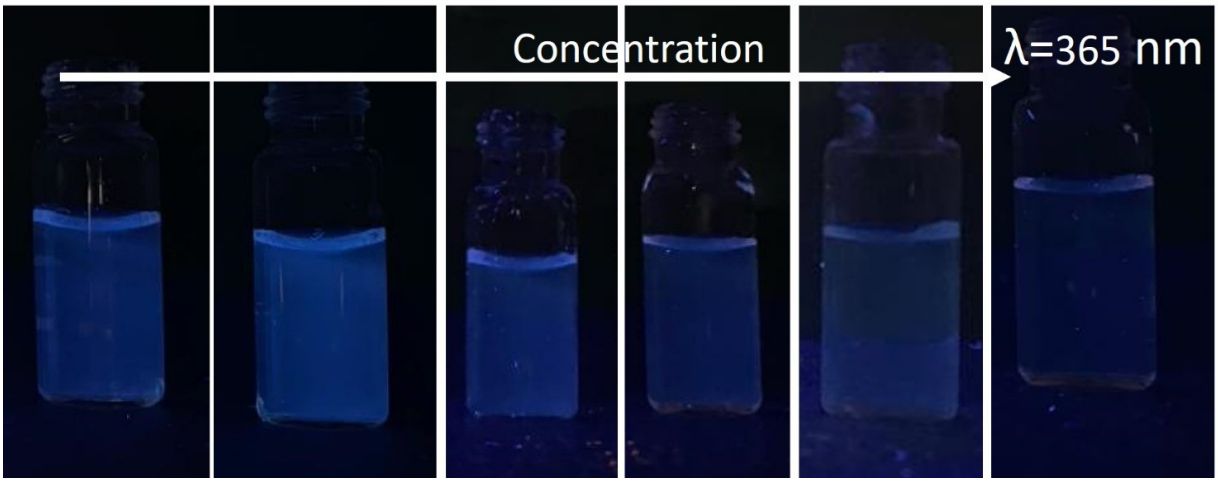

Concentration (mg/L)	Abs at 335 nm	Integrated fluorescence area
150	0.089	51618.301
100	0.074	48671.247
50	0.049	33119.876
30	0.023	15790.887
8	0.016	11049.823

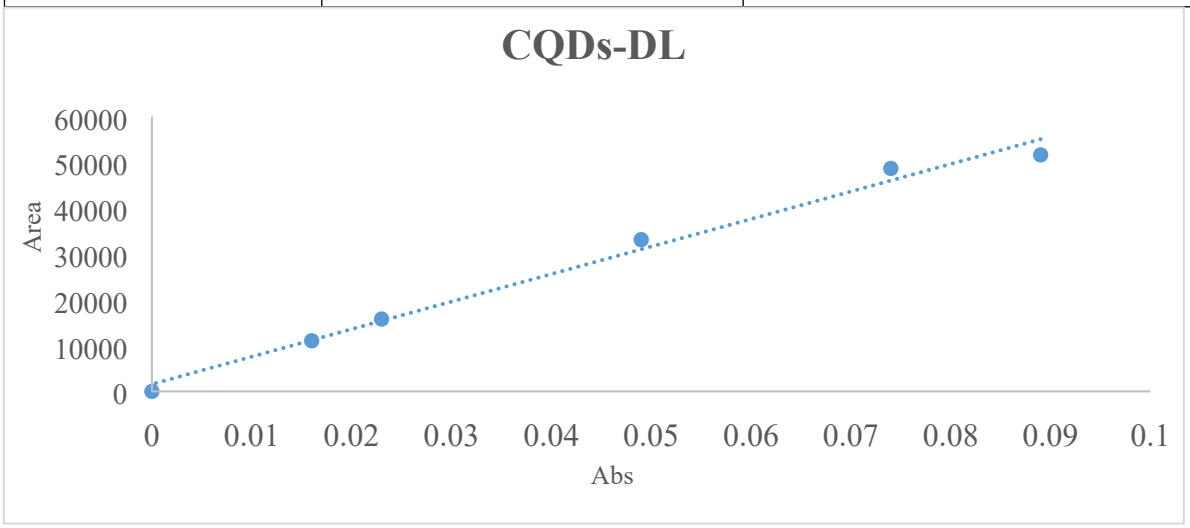

7. ICP-OES performance

The analysis of total mercury in natural water samples was performed using inductively coupled plasma optical emission spectrometry (ICP-OES), following the standardized methods SM 3030K and 3120B. This technique was selected due to its high sensitivity, precision, and ability to detect trace levels of mercury, making it ideal for evaluating the limits of detection (LOD) of the developed sensors. Additionally, critical parameters such as sample preparation, calibration protocols, and instrumental settings were carefully optimized to ensure accurate and reproducible results. The use of ICP-OES is particularly relevant in this context, as it provides reliable quantitative data essential for validating the sensors' performance and their potential applications[3] in environmental monitoring.

Table S 5. *Parameters used in the determination of ICP-OES.*

Parameter	units	value
Plasma gas flow	L/min	13
Auxiliary gas flow	L/min	0.2
Nebulizer gas flow	L/min	0.5
RF Power	W	1500
Pump flow rate	mL/min	1
Detection limit	mg/L	$25x10^{-5}$
Limit of quantification	mg/L	$50x10^{-5}$

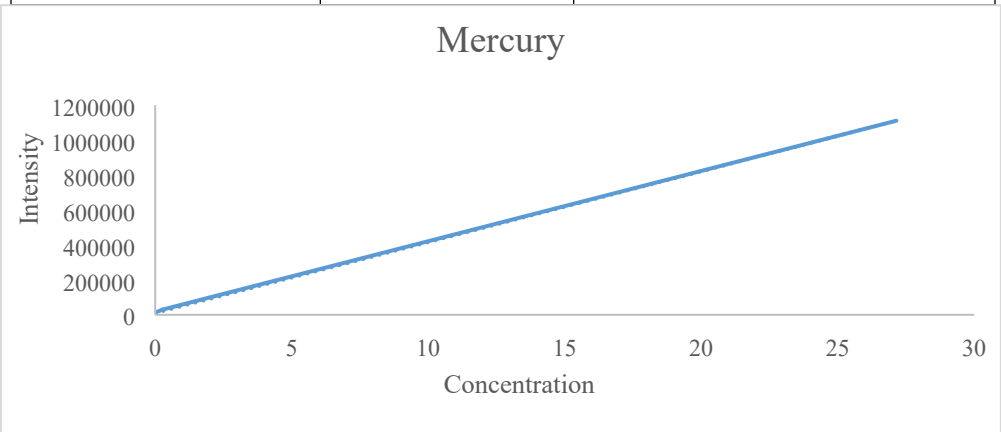

8. *Emission of TEMPO-oxidized cellulose nanofibers (TOCN)*

To rule out potential interference with the fluorescence signal of the biocomposites, the emission spectrum of TEMPO-oxidized cellulose nanofibers (TOCN) was recorded. The measurement was performed using an excitation wavelength of 530 nm. The resulting spectrum showed an emission peak centered at 570 nm, indicating that TOCN does not exhibit significant fluorescence in the spectral region of interest and therefore does not contribute to the observed fluorescence signal of the biocomposites (see Figure S11).

Figure S 11. *Emission spectrum of TEMPO-oxidized cellulose nanofibers (TOCN)*

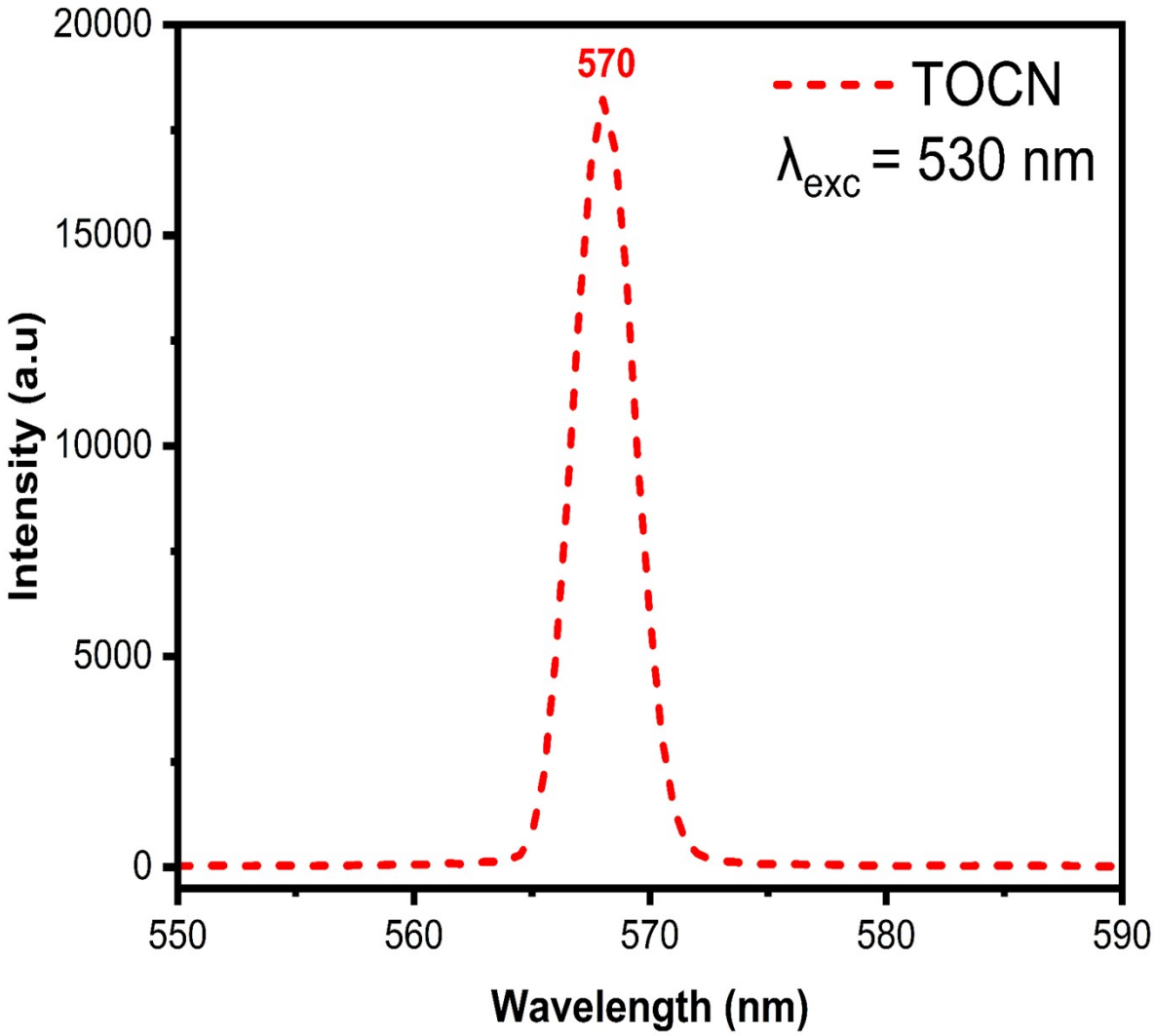

9. Stern-Volmer for fluorescence quenching of composites by Hg^{2+} ions.

Fluorescence quenching data were fitted using the modified Stern–Volmer model that accounts for both dynamic (□□) and static (□□) quenching contributions, as described by Equation 1. The nonlinear upward curvature observed in the I_o/I versus $[Hg^{2+}]$ plots support the coexistence of collisional interactions and ground-state complex formation[4]. The fit was performed over a semilogarithmic concentration range (0–27.2 mg/L of Hg^{2+}), excluding extreme concentrations to minimize signal saturation artifacts and enhance model accuracy.

Figure S 12. *Nonlinear Stern–Volmer plots for fluorescence quenching of composites by Hg^{2+} ions.*

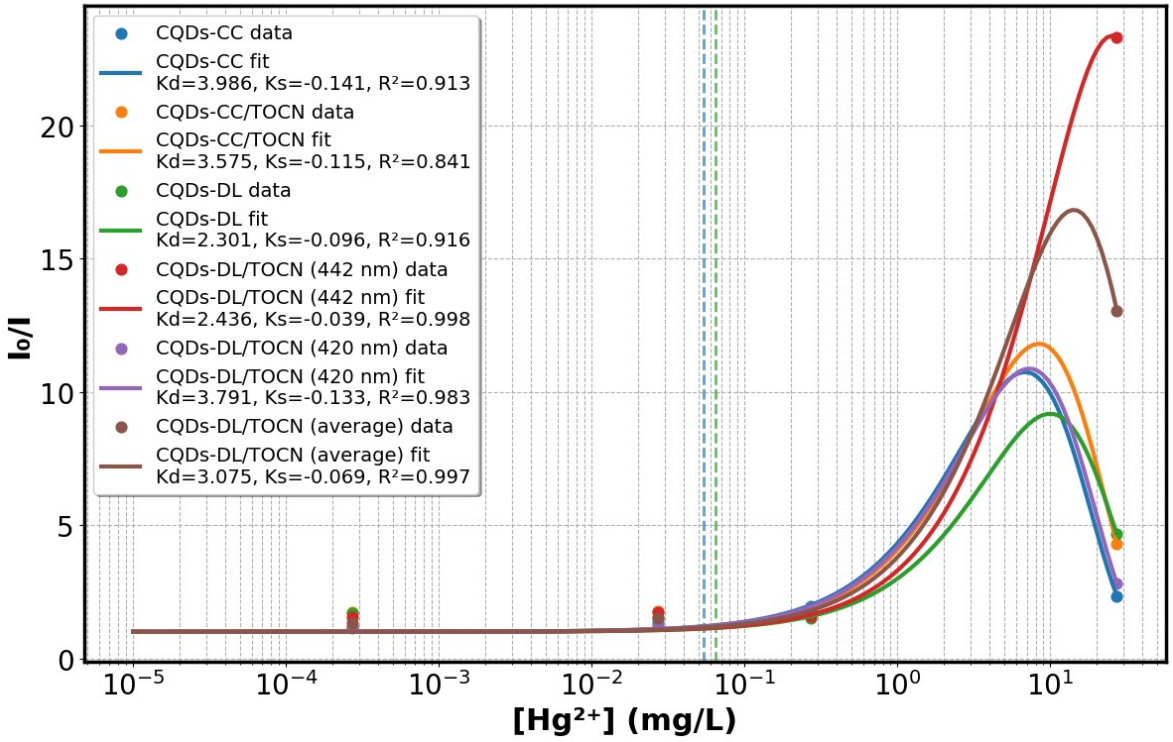

References

1. Y. Wang and A. Hu, *Emerging applications of carbon dots in catalysis, biology, and medicine*, J. Mater. Chem. C, *2014*, 2, 6921–6939.

2. J. R. Lachowicz, *Principles of Fluorescence Spectroscopy*, Springer, Boston, MA, 3rd edn, 2006, pp. 45-46.

3. M. Senila, A. Drolc, A. Pintar, L. Senila, and E. Levei, *Validation and measurement uncertainty evaluation of the ICP-OES method for the multi-elemental determination of essential and nonessential elements from medicinal plants and their aqueous extracts*, J. Anal. Sci. Technol., *2014*, 5, 37

4. Ciotta, E., Prosposito, P., & Pizzoferrato, R. (2019). Positive curvature in the Stern-Volmer plot is described by a generalized model for static quenching. Journal of Luminescence, 206, 518–522. https://doi.org/10.1016/j.jlumin.2018.10.106